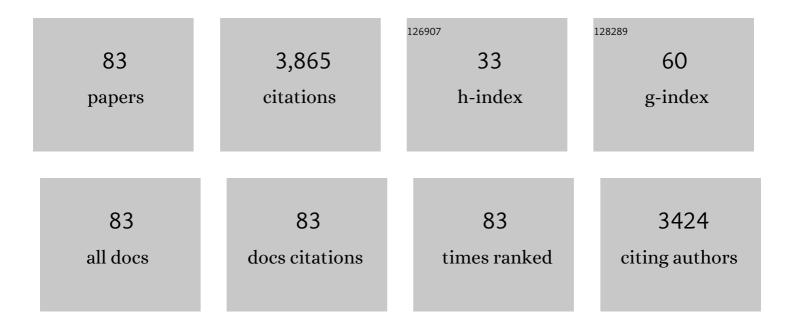
List of Publications by Year in descending order

Source: https://exaly.com/author-pdf/8805089/publications.pdf Version: 2024-02-01



Пхімс Гіц

#	Article	IF	CITATIONS
1	<scp><i>In situ</i></scp> encapsulated subnanometric <scp>CoO</scp> clusters within silicaliteâ€1 zeolite for efficient propane dehydrogenation. AICHE Journal, 2022, 68, e17451.	3.6	29
2	Multifunctional glass fibre filter modified with vertical graphene for one-step dynamic water filtration and disinfection. Journal of Materials Chemistry A, 2022, 10, 12125-12131.	10.3	4
3	Silicalite-1 Stabilizes Zn-Hydride Species for Efficient Propane Dehydrogenation. ACS Catalysis, 2022, 12, 5997-6006.	11.2	35
4	Optimal exposed crystal facets of α-Mn2O3 catalysts with enhancing catalytic performance for soot combustion. Catalysis Today, 2021, 376, 229-238.	4.4	22
5	Optimized Pt-MnOx interface in Pt-MnOx/3DOM-Al2O3 catalysts for enhancing catalytic soot combustion. Chinese Chemical Letters, 2021, 32, 1447-1450.	9.0	21
6	Biomass-derived nitrogen self-doped porous activation carbon as an effective bifunctional electrocatalysts. Chinese Chemical Letters, 2021, 32, 92-98.	9.0	25
7	Descriptor-Guided Design and Experimental Synthesis of Metal-Doped TiO ₂ for Propane Dehydrogenation. Industrial & Engineering Chemistry Research, 2021, 60, 1200-1209.	3.7	8
8	A hierarchical ZSM-22/PHTS composite material and its hydro-isomerization performance in hydro-upgrading of gasoline. Catalysis Science and Technology, 2021, 11, 5448-5459.	4.1	6
9	Hydrogen Clathrate Structures in Uranium Hydrides at High Pressures. ACS Omega, 2021, 6, 3946-3950.	3.5	3
10	Hierarchical Porous K-OMS-2/3DOM-m Ti _{0.7} Si _{0.3} O ₂ Catalysts for Soot Combustion: Easy Preparation, High Catalytic Activity, and Good Resistance to H ₂ O and SO ₂ . ACS Catalysis, 2021, 11, 5554-5571.	11.2	44
11	Taming the Redox Property of A _{0.5} Co _{2.5} O ₄ (A = Mg, Ca, Sr, Ba) toward High Catalytic Activity for N ₂ O Decomposition. ACS Applied Energy Materials, 2021, 4, 8496-8505.	5.1	17
12	Computational Screening and Experimental Synthesis of Doped TiO ₂ for Propane Dehydrogenation. Energy & Fuels, 2021, 35, 19624-19633.	5.1	5
13	Insight into the Potassium Poisoning Effect for Selective Catalytic Reduction of NO _{<i>x</i>} with NH ₃ over Fe/Beta. ACS Catalysis, 2021, 11, 14727-14739.	11.2	69
14	3DOM Mn-Based Perovskite Catalysts Modified by Potassium: Facile Synthesis and Excellent Catalytic Performance for Simultaneous Catalytic Elimination of Soot and NO _{<i>x</i>} from Diesel Engines. Journal of Physical Chemistry C, 2021, 125, 25545-25564.	3.1	16
15	Facile synthesis of 3D ordered macro-mesoporous Ce1-xZrxO2 catalysts with enhanced catalytic activity for soot oxidation. Catalysis Today, 2020, 355, 587-595.	4.4	14
16	Efficient Z-scheme photocatalysts of ultrathin g-C3N4-wrapped Au/TiO2-nanocrystals for enhanced visible-light-driven conversion of CO2 with H2O. Applied Catalysis B: Environmental, 2020, 263, 118314.	20.2	206
17	Trimetallic Catalyst Supported Zirconium-Modified Three-Dimensional Mesoporous Silica Material and Its Hydrodesulfurization Performance of Dibenzothiophene and 4,6-Dimethydibenzothiophene. Industrial & Engineering Chemistry Research, 2020, 59, 654-667.	3.7	18
18	Boosting the Removal of Diesel Soot Particles by the Optimal Exposed Crystal Facet of CeO ₂ in Au/CeO ₂ Catalysts. Environmental Science & Technology, 2020, 54, 2002-2011.	10.0	101

#	Article	IF	CITATIONS
19	Synthesis of highly ordered Al-Zr-SBA-16 composites and their application in dibenzothiophene hydrodesulfurization. Chemical Engineering Science, 2020, 213, 115415.	3.8	10
20	Deep Understanding of Strong Metal Interface Confinement: A Journey of Pd/FeO _{<i>x</i>} Catalysts. ACS Catalysis, 2020, 10, 8950-8959.	11.2	113
21	Z-scheme heterojunction of SnS2-decorated 3DOM-SrTiO3 for selectively photocatalytic CO2 reduction into CH4. Chinese Chemical Letters, 2020, 31, 2774-2778.	9.0	62
22	Transfer Hydrogenation of Fatty Acids on Cu/ZrO ₂ : Demystifying the Role of Carrier Structure and Metal–Support Interface. ACS Catalysis, 2020, 10, 9098-9108.	11.2	50
23	Breaking the scaling relationship <i>via</i> dual metal doping in a cobalt spinel for the OER: a computational prediction. Physical Chemistry Chemical Physics, 2020, 22, 18672-18680.	2.8	5
24	The surface structure of β-NiOOH (001) under reaction conditions and its effect on OER activity: An ab initio study. Molecular Catalysis, 2020, 493, 111082.	2.0	1
25	Hydrothermal Catalytic Upgrading of Model Compounds of Algae-Based Bio-Oil to Monocyclic Aromatic Hydrocarbons over Hierarchical HZSM-5. Industrial & Engineering Chemistry Research, 2020, 59, 20551-20560.	3.7	7
26	Ultra-small Ni(HCO ₃) ₂ as a water dissociation promoter boosting the alkaline hydrogen electrocatalysis performance of MoS ₂ . Chemical Communications, 2020, 56, 12065-12068.	4.1	5
27	Nickel–Iron Nitride–Nickel Sulfide Composites for Oxygen Evolution Electrocatalysis. ACS Applied Materials & Interfaces, 2020, 12, 41464-41470.	8.0	44
28	FeNi ₃ –FeNi ₃ N – a high-performance catalyst for overall water splitting. Sustainable Energy and Fuels, 2020, 4, 6245-6250.	4.9	5
29	SO ₂ -Tolerant Catalytic Removal of Soot Particles over 3D Ordered Macroporous Al ₂ O ₃ -Supported Binary Pt–Co Oxide Catalysts. Environmental Science & Technology, 2020, 54, 6947-6956.	10.0	42
30	Synergetic Effect of K Sites and Pt Nanoclusters in an Ordered Hierarchical Porous Pt-KMnO _{<i>x</i>} /Ce _{0.25} 2r _{0.75} O ₂ Catalyst for Boosting Soot Oxidation. ACS Catalysis, 2020, 10, 7123-7135.	11.2	47
31	Solvent-free rapid synthesis of porous CeWO _x by a mechanochemical self-assembly strategy for the abatement of NO _x . Journal of Materials Chemistry A, 2020, 8, 6717-6731.	10.3	42
32	Stabilizing platinum atoms on CeO2 oxygen vacancies by metal-support interaction induced interface distortion: Mechanism and application. Applied Catalysis B: Environmental, 2020, 278, 119304.	20.2	120
33	High-efficient non-noble metal catalysts of 3D ordered macroporous perovskite-type La2NiB'O6 for soot combustion: Insight into the synergistic effect of binary Ni and B' sites. Applied Catalysis B: Environmental, 2020, 275, 119108.	20.2	59
34	Amorphous MoS2 nanosheets on MoO2 films/Mo foil as free-standing electrode for synergetic electrocatalytic hydrogen evolution reaction. International Journal of Hydrogen Energy, 2020, 45, 17422-17433.	7.1	23
35	Multifunctional photocatalysts of Pt-decorated 3DOM perovskite-type SrTiO3 with enhanced CO2 adsorption and photoelectron enrichment for selective CO2 reduction with H2O to CH4. Journal of Catalysis, 2019, 377, 309-321.	6.2	114
36	Mechanochemical Synthesis of Highly Porous CeMnO <i>_x</i> Catalyst for the Removal of NO <i>_x</i> . Industrial & Engineering Chemistry Research, 2019, 58, 16472-16478.	3.7	16

#	Article	IF	CITATIONS
37	Roles of Surface-Active Oxygen Species on 3DOM Cobalt-Based Spinel Catalysts M _{<i>x</i>} Co _{3–<i>x</i>} O ₄ (M = Zn and Ni) for NO _{<i>x</i>} -Assisted Soot Oxidation. ACS Catalysis, 2019, 9, 7548-7567.	11.2	158
38	In-situ synthesis of ternary metal phosphides NixCo1â´'xP decorated Zn0.5Cd0.5S nanorods with significantly enhanced photocatalytic hydrogen production activity. Chemical Engineering Journal, 2019, 378, 122220.	12.7	55
39	The nature of Ni-O pairs for ethane activation on NiO(100) and NiO(110) surfaces. Molecular Catalysis, 2019, 474, 110417.	2.0	7
40	Role of oxygen vacancies and Mn sites in hierarchical Mn2O3/LaMnO3-l´ perovskite composites for aqueous organic pollutants decontamination. Applied Catalysis B: Environmental, 2019, 245, 546-554.	20.2	187
41	Roomâ€Temperature Photocatalytic Decomposition of N 2 O over Nanobeltâ€Like Bi 2 MoO 6. ChemistrySelect, 2019, 4, 5338-5344.	1.5	1
42	Novel photocatalyst incorporating Ni-Co layered double hydroxides with P-doped CdS for enhancing photocatalytic activity towards hydrogen evolution. Applied Catalysis B: Environmental, 2019, 254, 145-155.	20.2	209
43	Synthesis of Titanium Modified Three-Dimensional KIT-5 Mesoporous Support and Its Application of the Quinoline Hydrodenitrogenation. Energy & Fuels, 2019, 33, 5518-5528.	5.1	17
44	Enhanced activity and sulfur resistance for soot combustion on three-dimensionally ordered macroporous-mesoporous MnxCe1-xOÎ'/SiO2 catalysts. Applied Catalysis B: Environmental, 2019, 254, 246-259.	20.2	73
45	Interaction-Induced Self-Assembly of Au@La ₂ O ₃ Core–Shell Nanoparticles on La ₂ O ₂ CO ₃ Nanorods with Enhanced Catalytic Activity and Stability for Soot Oxidation. ACS Catalysis, 2019, 9, 3700-3715.	11.2	91
46	Three-dimensionally ordered macroporous K _{0.5} MnCeO _x /SiO ₂ catalysts: facile preparation and worthwhile catalytic performances for soot combustion. Catalysis Science and Technology, 2019, 9, 1372-1386.	4.1	27
47	Efficiently multifunctional catalysts of 3D ordered meso-macroporous Ce0.3Zr0.7O2-supported PdAu@CeO2 core-shell nanoparticles for soot oxidation: Synergetic effect of Pd-Au-CeO2 ternary components. Applied Catalysis B: Environmental, 2019, 251, 247-260.	20.2	105
48	Efficient Catalysts of La ₂ O ₃ Nanorod-Supported Pt Nanoparticles for Soot Oxidation: The Role of La ₂ O ₃ -{110} Facets. Industrial & Engineering Chemistry Research, 2019, 58, 7074-7084.	3.7	22
49	Experimental and DFT insights of BiVO4 as an effective photocatalytic catalyst for N2O decomposition. Chemical Engineering Journal, 2019, 366, 504-513.	12.7	33
50	Aluminum hydroxide-mediated synthesis of mesoporous metal oxides by a mechanochemical nanocasting strategy. Journal of Materials Chemistry A, 2019, 7, 22977-22985.	10.3	20
51	Green synthesis of mesoporous MnNbO _x oxide by a liquid induced self-assembly strategy for low-temperature removal of NO _x . Chemical Communications, 2019, 55, 15073-15076.	4.1	8
52	The effect of oxygen vacancies and water on HCHO catalytic oxidation over Co3O4 catalyst: A combination of density functional theory and microkinetic study. Chemical Engineering Journal, 2019, 355, 540-550.	12.7	69
53	Insights into the efficient adsorption of rhodamine B on tunable organo-vermiculites. Journal of Hazardous Materials, 2019, 366, 501-511.	12.4	86
54	Cu-SAPO-18 for NH ₃ -SCR Reaction: The Effect of Different Aging Temperatures on Cu ²⁺ Active Sites and Catalytic Performances. Industrial & Engineering Chemistry Research, 2019, 58, 2389-2395.	3.7	27

#	Article	IF	CITATIONS
55	BiMO _{<i>x</i>} Semiconductors as Catalysts for Photocatalytic Decomposition of N ₂ O: A Combination of Experimental and DFT+U Study. ACS Sustainable Chemistry and Engineering, 2019, 7, 2811-2820.	6.7	17
56	Defective Mn <i>_x</i> Zr _{1–<i>x</i>} O ₂ Solid Solution for the Catalytic Oxidation of Toluene: Insights into the Oxygen Vacancy Contribution. ACS Applied Materials & amp; Interfaces, 2019, 11, 730-739.	8.0	244
57	High-efficient catalysts of core-shell structured Pt@transition metal oxides (TMOs) supported on 3DOM-Al2O3 for soot oxidation: The effect of strong Pt-TMO interaction. Applied Catalysis B: Environmental, 2019, 244, 628-640.	20.2	111
58	Facet-dependent photocatalytic decomposition of N ₂ O on the anatase TiO ₂ : a DFT study. Nanoscale, 2018, 10, 6024-6038.	5.6	32
59	Study on Hydrodesulfurization of L/W Coexistence Zeolite Modified by Magnesium for FCC Gasoline. Energy & Fuels, 2018, 32, 777-786.	5.1	8
60	Density Functional Theory Study of the Formaldehyde Catalytic Oxidation Mechanism on a Au-Doped CeO2(111) Surface. Journal of Physical Chemistry C, 2018, 122, 438-448.	3.1	22
61	Combination of Density Functional Theory and Microkinetic Study to the Mn-Doped CeO ₂ Catalysts for CO Oxidation: A Case Study to Understand the Doping Metal Content. Journal of Physical Chemistry C, 2018, 122, 25290-25300.	3.1	16
62	Unraveling the structure–sensitivity of the photocatalytic decomposition of N ₂ O on CeO ₂ : a DFT+U study. Journal of Materials Chemistry A, 2018, 6, 19241-19255.	10.3	12
63	Carbonate-mediated Mars–van Krevelen mechanism for CO oxidation on cobalt-doped ceria catalysts: facet-dependence and coordination-dependence. Physical Chemistry Chemical Physics, 2018, 20, 16045-16059.	2.8	54
64	Enhancing the low temperature NH ₃ -SCR activity of FeTiO _x catalysts <i>via</i> Cu doping: a combination of experimental and theoretical study. RSC Advances, 2018, 8, 19301-19309.	3.6	10
65	Effect of Nb Promoter on the Structure and Performance of Iron Titanate Catalysts for the Selective Catalytic Reduction of NO with NH ₃ . Industrial & Engineering Chemistry Research, 2018, 57, 7802-7810.	3.7	26
66	Fe/Beta@Meso-CeO2 Nanostructure Core–Shell Catalyst: Remarkable Enhancement of Potassium Poisoning Resistance. Catalysis Surveys From Asia, 2018, 22, 181-194.	2.6	14
67	In Situ Synthesis of Strongly Coupled Co ₂ P-CdS Nanohybrids: An Effective Strategy To Regulate Photocatalytic Hydrogen Evolution Activity. ACS Sustainable Chemistry and Engineering, 2018, 6, 9940-9950.	6.7	61
68	Fabrication of Spinel-Type Pd _{<i>x</i>} Co _{3–<i>x</i>} O ₄ Binary Active Sites on 3D Ordered Meso-macroporous Ce-Zr-O ₂ with Enhanced Activity for Catalytic Soot Oxidation. ACS Catalysis, 2018, 8, 7915-7930.	11.2	157
69	Titanium-Modified TUD-1 Mesoporous Catalysts for the Hydrotreatment of FCC Diesel. Energy & Fuels, 2018, 32, 8210-8219.	5.1	10
70	Fe/Beta@SBAâ€15 coreâ€shell catalyst: Interface stable effect and propene poisoning resistance for no abatement. AICHE Journal, 2018, 64, 3967-3978.	3.6	51
71	Catalysts of 3D ordered macroporous ZrO ₂ -supported core–shell Pt@CeO _{2â^'x} nanoparticles: effect of the optimized Pt–CeO ₂ interface on improving the catalytic activity and stability of soot oxidation. Catalysis Science and Technology, 2017, 7. 968-981.	4.1	28
72	Selective catalytic reduction of NO with NH ₃ over Mo–Fe/beta catalysts: the effect of Mo loading amounts. RSC Advances, 2017, 7, 7130-7139.	3.6	28

#	Article	IF	CITATIONS
73	Catalysts of self-assembled Pt@CeO _{2â~î^} -rich core–shell nanoparticles on 3D ordered macroporous Ce _{1â~x} Zr _x O ₂ for soot oxidation: nanostructure-dependent catalytic activity. Nanoscale, 2017, 9, 4558-4571.	5.6	57
74	Mesoporous Co ₃ O ₄ supported Pt catalysts for low-temperature oxidation of acetylene. RSC Advances, 2017, 7, 18592-18600.	3.6	13
75	A Unique Fe/Beta@TiO ₂ Core–Shell Catalyst by Small-Grain Molecular Sieve as the Core and TiO ₂ Nanosize Thin Film as the Shell for the Removal of NO _{<i>x</i>} . Industrial & Engineering Chemistry Research, 2017, 56, 5833-5842.	3.7	24
76	Simultaneous NO _{<i>x</i>} and Particulate Matter Removal from Diesel Exhaust by Hierarchical Fe-Doped Ce–Zr Oxide. ACS Catalysis, 2017, 7, 3883-3892.	11.2	85
77	Synthesis of micro-mesoporous materials ZSM-5/FDU-12 and the performance of dibenzothiophene hydrodesulfurization. RSC Advances, 2017, 7, 28038-28047.	3.6	32
78	The simultaneous purification of PM and NOx in diesel engine exhausts over a single 3DOM Ce _{0.9â´'x} Fe _{0.1} Zr _x O ₂ catalyst. Environmental Science: Nano, 2017, 4, 1168-1177.	4.3	27
79	Feâ€Beta@CeO ₂ coreâ€shell catalyst with tunable shell thickness for selective catalytic reduction of NO _{<i>x</i>} with NH ₃ . AICHE Journal, 2017, 63, 4430-4441.	3.6	51
80	Mechanistic Study of Selective Catalytic Reduction of NO _{<i>x</i>} with NH ₃ over Mn-TiO ₂ : A Combination of Experimental and DFT Study. Journal of Physical Chemistry C, 2017, 121, 19859-19871.	3.1	47
81	Restricted diffusion of model sulfides over a NiMo/BK catalyst under hydrodesulfurization reaction conditions. RSC Advances, 2017, 7, 44340-44347.	3.6	7
82	The catalytic performances and reaction mechanism of nanoparticle Cd/Ce–Ti oxide catalysts for NH ₃ -SCR reaction. RSC Advances, 2017, 7, 50127-50134.	3.6	11
83	Simultaneous removal of PM and NO _x over highly efficient 3DOM W/Ce _{0.8} Zr _{0.2} O ₂ catalysts. RSC Advances, 2017, 7, 56509-56518.	3.6	7